Study of Anodic Electrodeposition of CeO$_2$ Thin Film Using Electrochemical Noise Technique

Yang Yang [1,2,3], *Yu Chen* [2,3,*], *Xiao-qing Du* [3], *Song Feng* [1], *Zhao Zhang* [3]

[1] School of Materials Science and Engineering, Guizhou Minzu University, Guiyang 550025, P. R. China
[2] College of Chemistry & Chemical Engineering, Binzhou University, Binzhou, Shandong 256603, P. R. China
[3] Department of Chemistry, Zhejiang University, Hangzhou 310027, P. R. China
[*]E-mail: chen123yu123@163.com

The anodic electrodeposition of CeO$_2$ thin film was studied by means of cyclic voltammetry (CV), electrochemical noise (EN) analysis, scanning electron microscopy (SEM) and XRD. The CV results reveal that the electroplating behavior of CeO$_2$ on 316L stainless electrode is mainly electrochemical-controlled. It is found that the potential moves in the positive direction slowly when the electroplating current density (J_k) is small (0.01-0.05 mA·cm^{-2}) and moves quickly in the positive direction to reach a plateau in the case of much larger J_k value, suggesting a progressive and instantaneous nucleation/growth mechanism, respectively. New parameters are proposed from EN analysis to investigate the relationship between the EN feature and the CeO$_2$ thin film structure. It is interesting to infer that parameter n_2 presented the same variation trend with the crystallite size from the XRD measurements with the electroplating current density.

1. INTRODUCTION

CeO$_2$ (Ceria) is a rare earth oxide that has a wide range of applications due to its particular 4f structure ([Xe]4f^1) and its ability to store, release or transport oxygen and oxygen ion. For example, cerias have been used as ionic conductors in solid oxide fuel cells (SOFC) [1], polishing agents for chemical mechanical and planarization (CMP) processes [2], catalysts for the three-way catalysis (TWC) of exhaust gas from automobiles [3], and coatings for the corrosion protection of metallic materials [4-8].

It is known that ceria powders or coatings can be prepared using chemical vapor deposition [9,10], electroplating [11-15], hydrothermal precipitation [16,17], sol-gel methods [18] and many other techniques. Among them, electroplating is a promising method for the preparation of films and possesses many advantages, such as low processing temperature, normal handling pressure, simple operation and high purity of deposits [19]. There have been many studies of the electrodeposition of cerium oxide films in aqueous electrolyte [20-22]. However, most of them have focused on either the surface structure [23,24] or the application of ceria films [25,26] and few studies have reported on the nucleation and growth mechanism.

It has been reported previously [27-30] that during metal electrodeposition, electrocrystallization electrochemical noise (EEN) can be used as "fingerprints" to characterize the electrodeposition process and the deposit structure, and the EN analysis can supply more detailed information about the deposit structure than other normal electrochemical measurements (such as cyclic voltammogram, chronoamperometry and electrochemical impedance spectroscopy). However, no literature has reported the electrodeposition behavior of CeO_2 thin film on 316L stainless steel using the EN analysis.

The goal of this work is to systematically study the electrodeposition process of CeO_2 on 316L stainless steel with cyclic voltammetry (CV), electrochemical noise (EN) analysis, scanning electron microscopy (SEM) and XRD and more specifically, to investigate the correlations between the EN features of CeO_2 electrodeposition process and the deposited structure.

2. EXPERIMENTAL

2.1. Materials

An electroplating bath consisting of 0.05 M $Ce(NO_3)_3 \cdot 6H_2O$ (Analytical reagent (AR), 0.1 M CH_3COONH_4 (AR) as a complex agent, 10 % (V) CH_3CH_2OH (AR) and double-distilled water that was further purified with a Milli-Q purification system (Millipore, resistivity, 18.2 MΩ cm). All electroplating solutions are naturally aerated unless otherwise specified.

A 316L stainless steel rod (SS, working area 0.50 cm^2) was adopted as the working electrode for the electrochemical measurements. Before each experiment, the working surface was polished to mirror quality using a 2.5 μm diamond paste and then rinsed with acetone and double-distilled water. The treated steel was dried with nitrogen gas (N_2) and then dipped into the electrochemical cell for use. A saturated calomel electrode (SCE) connected through a salt bridge was used as reference, and a large platinum foil (25 × 25 × 0.2 mm) was used as counter electrode. All potentials were referenced to an SCE unless otherwise stated.

2.2. Electrochemical experiment

A classical 3-electrode cell was used in the electrochemical experiments. CV measurements were carried out using a commercial Model 660A electrochemical analyzer/workstation (CH

Instruments Inc., US). EEN tests were conducted at different electroplating current densities with a commercial PowerLab coupled with GP Amp (ADInstruments Pty Ltd., Australia) at a sampling rate of 10 Hz. All the measurements were performed in a quiescent solution. The deposition bath temperature was controlled by a thermostat water tank at 50 ± 0.5 °C and the experimental device was shielded in a Faradaic cage.

2.3. Surface analysis

The surface morphologies were observed using scanning electron microscopy (SEM, Hitachi SU70). The structure and phase composition were identified by X-ray diffraction (XRD). The XRD analysis was conducted with a RIGAKU D/MAX 2550 diffractometer using Cu *K*a radiation (λ = 0.154056 nm) at a scan rate of 5 °/ min, the tube source was operated at 40 kV and 250 mA.
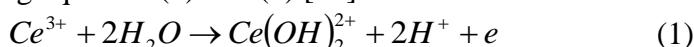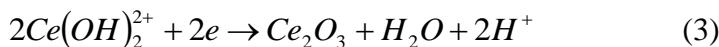
3. RESULTS AND DISCUSSION

3.1 CV measurements
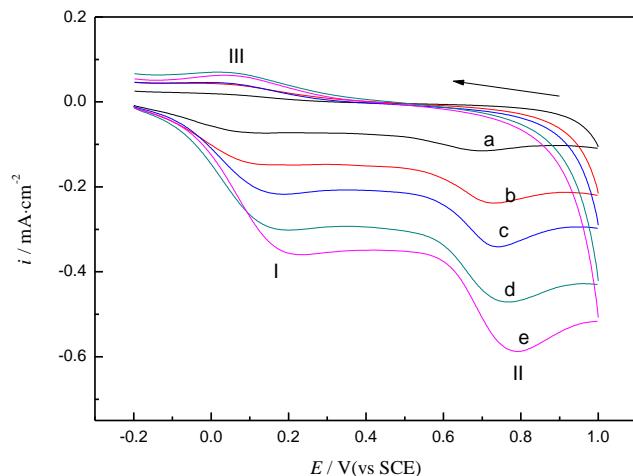
Figure 1. The cyclic voltammetry curves of 316L SS at different scan rate in deposition bath containing 50 mM Ce^{3+}, a: 20 mV/s, b: 40 mV/s, c: 60 mV/s, d: 80 mV/s, e: 100 mV/s.

The electroplating behavior of CeO$_2$ on 316L stainless electrode was first investigated using CV at different scan rate as shown in **Fig. 1**. There are two anodic peaks (I and II) and one cathodic peak (III). One anodic peak at approximately 0.17 V corresponds to the anodic dissolution of the 316L substrate; another anodic peak located at 0.78 V is attributed to the oxidation of Ce^{3+} ions according to equation (1) which shifts in the positive direction with increasing scan rate. In addition, the cathodic peak located at approximately 0.05 V can be assigned to the partial reduction of the ceria film following equation (2) and (3) [31].

$$Ce^{3+} + 2H_2O \rightarrow Ce(OH)_2^{2+} + 2H^+ + e \qquad (1)$$

$$CeO_2 + 2H^+ \rightarrow Ce(OH)_2^{2+} \qquad (2)$$

$$2Ce(OH)_2^{2+} + 2e \rightarrow Ce_2O_3 + H_2O + 2H^+ \qquad (3)$$

The peak current density of peak II is associated with the complete consumption of Ce^{3+} ions at the electrode surface, and the peak current density increases with increasing scan rate. The rising section of the current peak starting from 0.56 V is mainly assigned to the nucleation/growth processes of CeO_2 crystallites, and the descending section originates from the diffusion.

In previous studies [32–34], a linear dependence of the peak current density on the square root of the potential scan rate was shown satisfied according to the Randles-Sevcik equation when the electrodeposition process is diffusion-controlled and is given as follows:

$$j_p = 2.69 \times 10^5 z^{1.5} D^{0.5} v^{0.5} c \qquad (4)$$

where j_p is the peak current density, z is the number of electrons, D is the diffusion coefficient of Ce^{3+} ions, v is the potential scan rate and c is the bulk concentration of Ce^{3+} ions.

Fig. 2 shows the correlation between the peak current density and the square root of the potential scan rate. Clearly, the correlation coefficient is calculated to be 0.97, indicating that the electroplating behavior of the CeO_2 thin film on the 316L stainless electrode is not diffusion-controlled. This phenomenon that the anodic oxidation process of Ce^{3+} is mainly electrochemically controlled has been reported in the literature [35]. The reason may be that CeO_2 is a semiconductor with poor conductivity, which will slow the further oxidation when the surface was electrodeposited with a CeO_2 thin film, causing electrochemically controlled electroplating process.
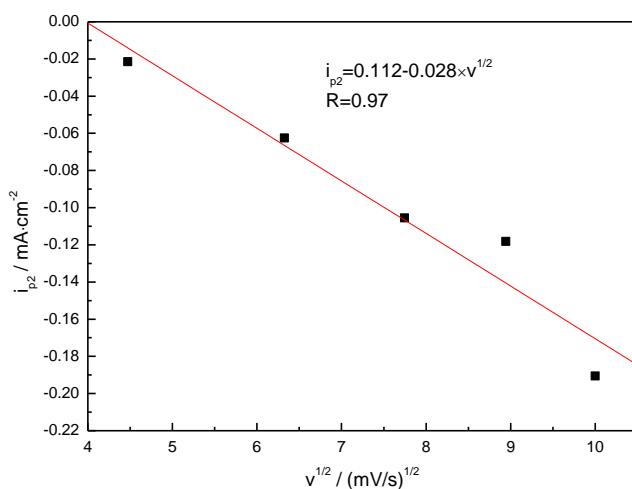

Figure 2. The plots of $i_{p(II)}$ vs $v^{1/2}$ and the fitted results

3.2 Electrochemical noise

Fig.3 shows the potential EN in the initial 120 s for CeO_2 electroplating onto 316L stainless steel at different current densities. The potential EN curves present different features at different electroplating current densities (J_k). When the electroplating current density is small (0.01-0.05 mA·cm^{-2}), the potential moves slowly in the positive direction, which may be attributed to the combined action of the 316L substrate and the CeO_2 particles according to the mixed potential theory

[36] in addition to the influence of electric double layer charging process. Meanwhile, the slow movement of the potential also reflects the slow nucleation/growth rate of the CeO_2 thin film at this low current density. In the case of much larger J_k value, from 0.25 mA cm^{-2} to 1.5 mA cm^{-2}, the potential initially moves quickly in the positive direction and then reaches a plateau, suggesting a quick nucleation process. From **Fig.3**, it is apparent that the larger J_k value is, the more positive the value of the final stable potential is, and less time is required to reach the potential plateau. The higher the electroplating current density J_k is, the sooner Ce^{3+} is consumed at the 316L electrode surface. Furthermore, it is inferred that the electroplating process exhibits an instantaneous nucleation/growth mechanism at high electroplating current densities (0.5 - 1.5 mA cm^{-2}) and progressive nucleation/growth mechanism at low electroplating current densities (0.01 – 0.25 mA cm^{-2}) [37].
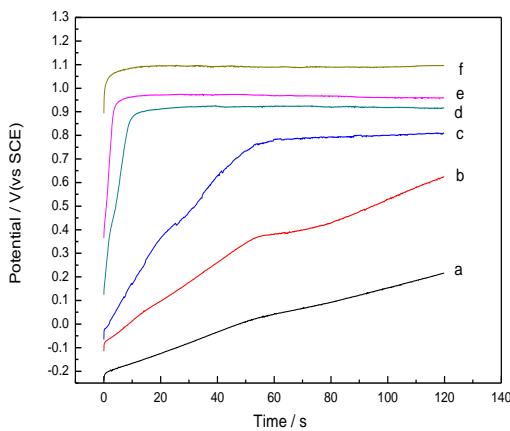
Figure 3. Potential EEN for CeO_2 thin film electroplating at different current densities, a: 0.01 mA·cm^{-2}, b: 0.025 mA·cm^{-2}, c: 0.05mA·cm^{-2}, d: 0.25 mA·cm^{-2}, e: 0.5 mA·cm^{-2}, f: 1.5 mA·cm^{-2}

The potential EN data containing 5120 points selected after the initial 10 ms of the double layer charging process are analyzed with wavelet analysis [38] using the orthogonal Daubechies wavelets (FWT) of the fourth order (db4). For FWT analysis, the interval range of each crystal is given by:

$$(C_1^l, C_2^l) = (2^l \Delta t, 2^{l-1} \Delta t) \qquad (5)$$

The overall energy (E) of the noise containing 5120 data points in this experiment is calculated as follows:

$$E = \sum_{n=1}^{N} S_n^2 (n = 1,2,...,N, N = 5120) \qquad (6)$$

Then, the fraction of the energy associated with each crystal (D and S) can be calculated as follows:

$$E_l^D = \frac{1}{E} \sum_{k=1}^{N/2^l} D_{l,k}^2 (l = 1,2,...,J, J = 8) \qquad (7)$$

$$E_J^S = \frac{1}{E} \sum_{k=1}^{N/2^l} S_{J,k}^2 (l = 1,2,...,J) \qquad (8)$$

Since the chosen wavelets are orthogonal, the following equation is satisfied [39]:

$$E = E_J^S + \sum_{l=1}^{J} E_l^D \qquad (9)$$

An energy distribution plot (EDP) is used to describe the relationship between the relative energy accumulated by each crystal and the crystal name. Furthermore, the EDP is re-plotted by discounting the contribution of the S_8 crystal from the ensemble signal energy to eliminate the energy contribution of DC drift from the ensemble energy of the noise (the re-plotted EDP is named as RP-EDP).
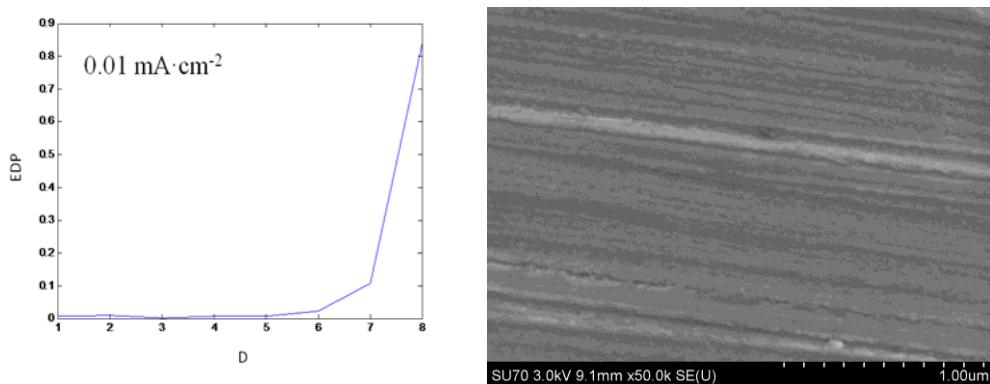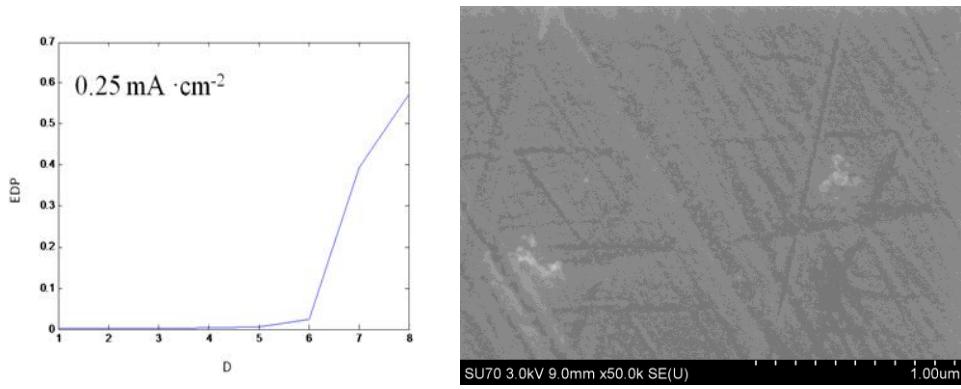

Figure 4. RP-EDP generated during CeO_2 thin film electroplating and the corresponding SEM image of deposit (J_k=0.01 mA cm^{-2}, t = 120 s).
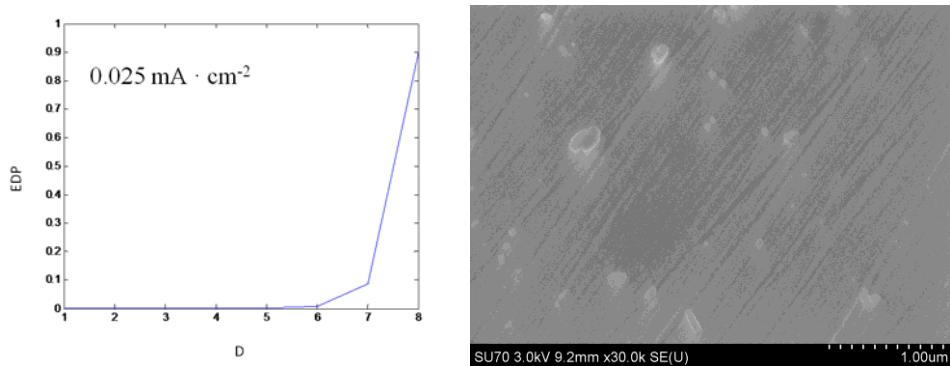
Figure 5. RP-EDP generated during CeO_2 thin film electroplating and the corresponding SEM image of deposit (J_k=0.025 mA cm^{-2}, t = 120 s).
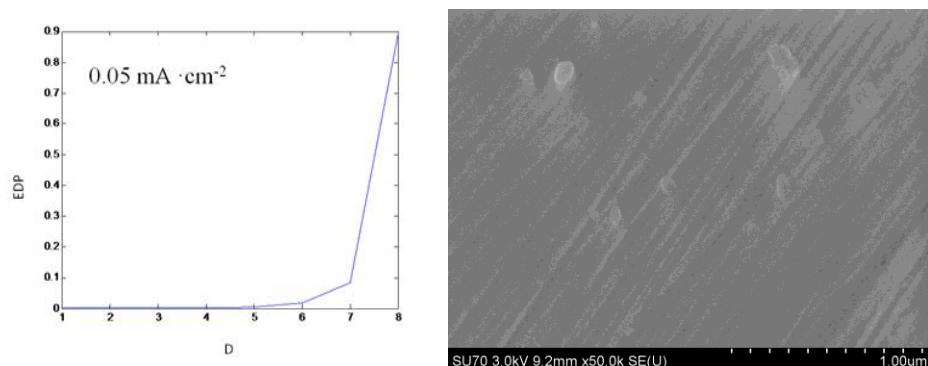
Figure 6. RP-EDP generated during CeO_2 thin film electroplating and the corresponding SEM image of deposit (J_k=0.05 mA cm^{-2}, t = 120 s).

Figure 7. RP-EDP generated during CeO_2 thin film electroplating and the corresponding SEM image of deposit (J_k=0.25 mA cm^{-2}, t = 120 s).
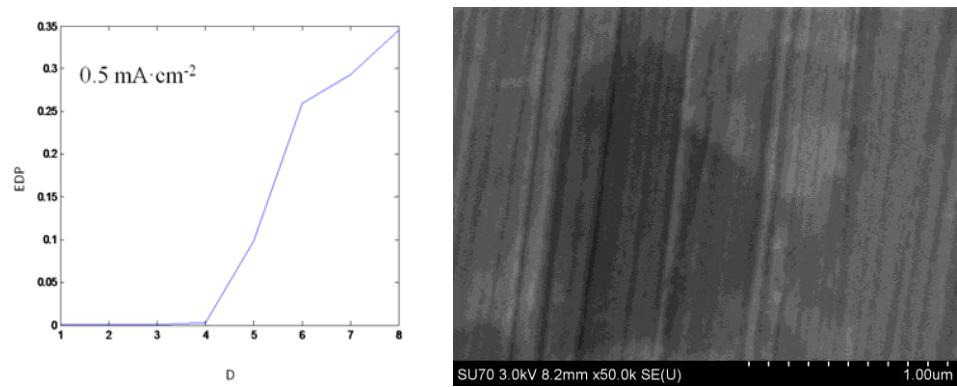

Figure 8. RP-EDP generated during CeO_2 thin film electroplating and the corresponding SEM image of deposit (J_k=0.5 mA cm^{-2}, t = 120 s).
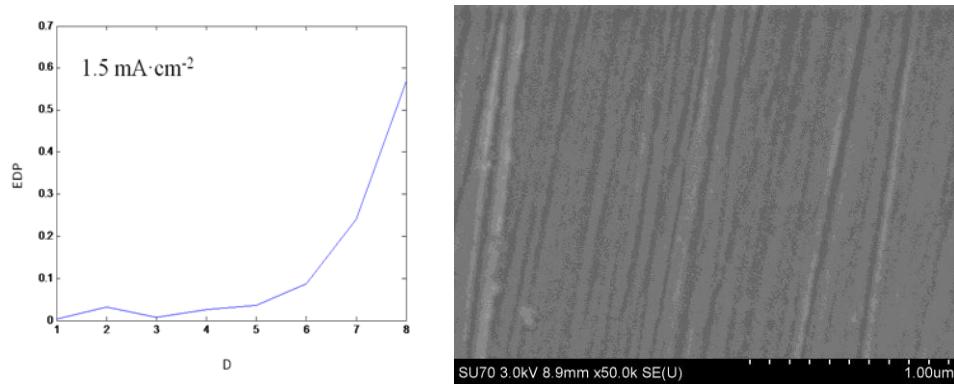

Figure 9. RP-EDP generated during CeO_2 thin film electroplating and the corresponding SEM image of deposit (J_k=1.5 mA cm^{-2}, t = 120 s).

According to previous studies [40-42], the RP-EDP can be divided into three segments: 1) region A between D_1 and D_3, which mainly characterizes the nucleation process, 2) region B between D_3 and D_6, which mainly characterizes the growth process, and 3) region C between D_6 and D_8, which mainly reflects the information about the diffusion process.

To investigate the correlations between the EN features of CeO_2 electroplating process and the film structure, the obtained RP-EDP plots and the corresponding CeO_2 deposit morphologies at a 120 s deposition time at different J_k values are plotted in **Figs. 4-9**.

According to Zhang [43], the obtained RP-EDPs supplied useful information about the dominant corrosion step of the AZ91D alloy, in which the position of the maximum relative energy in RP-EDP was related to the dominant process in all events, which drifts from crystal d_8 through d_3 to d_1, revealing three different corrosion stages during AZ91D alloy corrosion at different immersion time. Meanwhile, the RP-EDP can also be used as "fingerprints" to characterize the electrodeposition process and the deposit structure [44] based on the phenomenon that the maximum value of the RP-EDP obtained from FWT drifted from a region with a lower frequency range to a region with a higher frequency range, representing different dominant electrodeposition processes at different electrodeposition current densities, and the corresponding material structure changed from dendritic to compact.

Unfortunately, the characteristic of the RP-EDP plots generated during CeO_2 electroplating process with different electroplating current densities, as shown in **Fig.4-9**, are rather obscure; the energy is mainly deposited in the low frequency domain (region C, **Table 1**), suggesting that the CeO_2 electroplating process is controlled by the nucleation/growth step. Thus, it is difficult to evaluate the relationship between the RP-EDP features and the CeO_2 thin film structure from **Fig.4-9** in our measurements.

To analyze the relationship between the RP-EDP features and the surface structure of the CeO_2 thin film, the CeO_2 thin film structures are also characterized using XRD (**Fig.11**), and two new parameters (n_1 or $n_1^{'}$ and n_2) are defined to differentiate the nucleation and growth processes as follows:

$$n_1 = \frac{E_{d1} + E_{d2} + E_{d3}}{E_{d4} + E_{d5} + E_{d6}} \qquad (10)$$

$$n_1^{'} = \frac{E_{d1} + E_{d2} + E_{d3}}{E_{d1} + E_{d2} + E_{d3} + E_{d4} + E_{d5} + E_{d6}} \qquad (11)$$

$$n_2 = \frac{E_{d4} + E_{d5} + E_{d6}}{E_{d1} + E_{d2} + E_{d3} + E_{d4} + E_{d5} + E_{d6}} \qquad (12)$$

where $Ed1+Ed2+Ed3$ is the nucleation energy defined in region A, and $Ed4+Ed5+Ed6$ corresponds to the growth energy in region B.

The relationship of the three new parameters n_1 ($n_1^{'}$) and n_2 with a CeO_2 thin film electroplating current density is plotted in **Fig.10**. It can be seen that the variation of these parameters (n_1 or $n_1^{'}$ and n_2) with electroplating current density can be classified into two parts (**Fig.10**): (a) In the case of low J_k value (0.01 mA·cm^{-2} - 0.25 mA·cm^{-2}), both n_1 and $n_1^{'}$ decrease with increasing J_k. (b) In the case of higher J_k values (0.5 mA·cm^{-2} – 1.5 mA·cm^{-2}), both n_1 and $n_1^{'}$ increase with increasing J_k. During the whole electroplating current density range, trend of n_2 is always opposite to both n_1 and $n_1^{'}$.

Table 1. The RP-EDP results of CeO_2 thin film electroplating at different current densities

$i/mA \cdot cm^{-2}$	0.01	0.025	0.05	0.25	0.5	1.5
E_{d1}	2.46×10^{-6}	5.61×10^{-7}	4.85×10^{-7}	1.64×10^{-7}	1.24×10^{-7}	1.76×10^{-7}
E_{d2}	3.31×10^{-6}	1.54×10^{-6}	1.33×10^{-6}	4.60×10^{-7}	6.79×10^{-7}	1.69×10^{-6}
E_{d3}	9.26×10^{-7}	4.07×10^{-7}	6.17×10^{-7}	8.76×10^{-7}	7.73×10^{-7}	4.19×10^{-7}
E_{d4}	2.16×10^{-6}	8.43×10^{-7}	1.67×10^{-6}	1.05×10^{-5}	5.24×10^{-6}	1.33×10^{-6}
E_{d5}	2.24×10^{-6}	7.35×10^{-7}	3.05×10^{-6}	2.44×10^{-5}	1.73×10^{-4}	1.85×10^{-6}
E_{d6}	8.74×10^{-6}	4.43×10^{-6}	1.68×10^{-5}	1.24×10^{-4}	4.56×10^{-4}	4.59×10^{-6}
E_{d7}	4.02×10^{-5}	5.55×10^{-5}	8.27×10^{-5}	0.002	5.15×10^{-4}	1.27×10^{-5}
E_{d8}	3.14×10^{-4}	5.78×10^{-4}	8.86×10^{-4}	0.0029	6.08×10^{-4}	3.00×10^{-5}
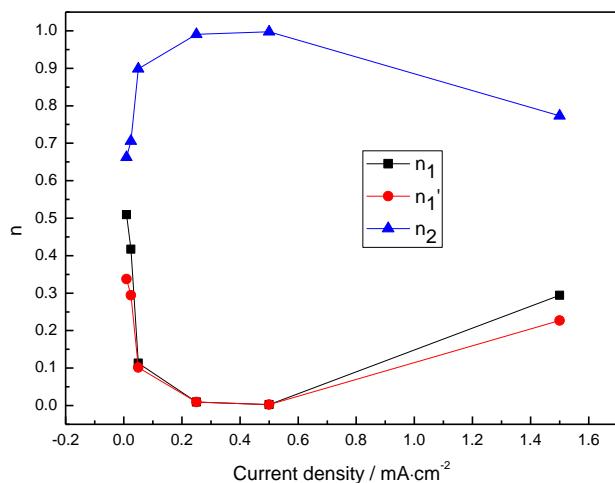
Figure 10. The dependence of the parameters n_1, n_1' and n_2 on current density
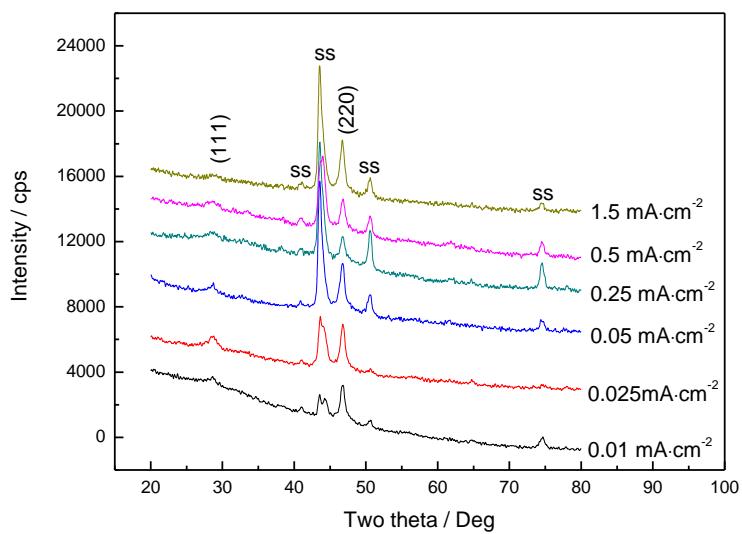
Figure 11. The XRD patterns of CeO_2 thin films deposited at different current density.

Fig.11 shows the typical XRD patterns of CeO_2 thin films deposited at different current densities. Most of the peaks can be assigned to those of CeO_2 (PDF No. 34-0394). The peak for the (2

2 0) plane is the most intense, and the peak assigned to the (1 1 1) plane has a weak intensity, indicating that the electrodeposited CeO_2 thin films are deposited preferentially in the (2 2 0) plane in this range of current densities. The mean crystallite size of the deposits is calculated using Scherrer's formula [23]:

$$D = \frac{k\lambda}{\beta \cos\theta} \qquad (11)$$

where D is the crystallite size, k is a constant (0.9 for Gaussian line profiles and small cubic crystals of uniform size), λ is the wavelength of the X-rays, θ is the diffraction angle, and β is the corrected full width at half maximum of the peak. The analyzed average crystallite size ($\overline{D}$) of the CeO_2 thin film are listed in **Table 2**.

Table 2. The average crystallite size of the CeO_2 thin films in different deposition current densities

$i/mA \cdot cm^{-2}$	0.01	0.025	0.05	0.25	0.5	1.5
$\overline{D}$ / nm	11.1	11.5	11.7	12.1	13.1	12.4

It is noticeable that the crystallite size ($\overline{D}$) (**Table 2**) shows the same trend as n_2 (**Fig.10**) versus the electroplating current density. Briefly, the value of $\overline{D}$ first increases with increasing J_k value and then decreases when J_k increases from 0.5 mA cm^{-2} to 1.5 mA cm^{-2}. The CeO_2 thin film formation process consist of both the nucleation and growth reactions and the latter always competes with the former. Meanwhile, it is known that nucleation always occurs prior to the growth of the crystallite [45]. Thus, the relative rate plays an important role on the value of $\overline{D}$. Generally, a higher nucleation rate and lower growth rate of the crystallites together result in a smaller $\overline{D}$ [46]. When the J_k value is low (0.01 mA cm^{-2} to 0.5 mA cm^{-2}), the CeO_2 thin film electroplating process is electrochemically controlled and follows a progressive nucleation/growth mechanism. Few nuclei can be formed on the heterogeneous or foreign substrate because their formation requires a much higher activation energy, and consequently the value of $\overline{D}$ is smaller. As the J_k value increases, the active points on the substrate become larger, and CeO_2 crystallites can nucleate more easily on the 316L stainless substrate surface. The higher electroplating current density will facilitate the growth of CeO_2 crystallites, resulting in a larger value of $\overline{D}$. When the electroplating current density is high enough (larger than 0. 5 mA.cm^{-2}), the CeO_2 thin film electroplating process mainly occurs as an instantaneous nucleation/growth mechanism and the CeO_2 crystallites can be instantaneously nucleate on the entire 316L substrate surface. Meanwhile, O_2 forms on the 316L electrode surface from water electrolysis because the stable potential at the plateau position (**Fig.3**) is more positive than the water electrolysis potential, and its formation accelerates the CeO_2 crystallites nucleation rate. Therefore, the value of n_2 decreases as the electroplating current density increases.

4. CONCLUSIONS

Cyclic voltammetry (CV), electrochemical noise (EN) analysis, scanning electron microscopy (SEM) and XRD were used to investigate the anodic electrodeposition process of CeO_2 thin film. The

CV results reveal that the electroplating behavior of CeO_2 on a 316L stainless steel electrode is mainly electrochemically-controlled. EN measurements show that the potential moves in the positive direction slowly when the electroplating current density (J_k) is small, whereas it moves quickly in the positive direction and then reaches a plateau in the case of much larger J_k values. New parameters are proposed from the EN analysis to understand the relationship between the EN feature and the CeO_2 thin film structure. Interestingly, parameter n_2 presented the same variation trend with the crystallite size with respect to the electroplating current density which can be separated into two parts: (a) when the current density is relatively low, n_2 increases with increasing the current densities and (b) when the current density is relatively high (increasing from 0.5 mA cm^{-2} to 1.5 mA cm^{-2}), n_2 decreases to a smaller value.

References

1. E.P. Murray, T. Tsai and S.A. Barnett, *Nature,* 400 (1999) 649.
2. X.D. Feng, D.C. Sayle, Z.L. Wang, M.S. Paras, B.Santoral, A.C. Sutorik, T.T. Sayle, Y. Yang, Y. Ding, X.D. Wang and Y.S. Her, *Science,* 312 (2006) 1504.
3. R.D. Monte and J. Kašpar, *J. Mater. Chem.,* 15 (2005) 633.
4. X.W. Yu, C.N. Cao, Z.M. Yao, D.R. Zhou and Z.D. Yin, *Corros. Sci.,* 43 (2001) 1283.
5. H.Y. Su, W.J. Li and C.S. Lin, *J. Electrochem. Soc.,* 159 (2012) C219.
6. Y. Hamlaoui, C. Rémazeilles, M. Bordes, L. Tifouti and F. Pedraza, *Corros. Sci.,* 52 (2010) 1020.
7. S.T. Aruna, C.N. Bindu, V. Ezhil Selvi, V.K. William Grips and K.S. Rajam, *Surf. Coat. Technol.,* 200 (2006) 6871.
8. M.F. Montemor and M.G.S. Ferreira, *Electrochim. Acta,* 52 (2007) 6976.
9. J.F. Jue, J. Jesko and A.V. Virkar, *J. Electrochem. Soc.,* 139 (1992) 2458.
10. M. Capitan, A. Paul, J. Pastol and J. Odriozola, *Oxid. Met.,* 52 (1999) 447.
11. J.A. Switzer, *Am. Ceram. Soc. Bull.,* 66 (1987) 1521.
12. Y. Zhou and J.A. Switzer, *J. Alloys Compd.,* 237 (1996) 1.
13. T.D. Golden and A.Q. Wang, *J. Electrochem. Soc.,* 150 (2003) C621.
14. A.Q. Wang and T.D. Golden, *J. Electrochem. Soc.,* 150 (2003) C616.
15. A.Q. Wang, P. Punchaipetch, R.M. Wallace and T.D. Golden, *J. Vac. Sci. Techno.,* B 21 (2003) 1169.
16. M. Hirano, E. Kato, *J. Am. Ceram. Soc.* 79 (1996) 777.
17. M. Hirano, E. Kato, *J. Am. Ceram. Soc.* 82 (1999) 786.
18. N. Özer, *Sol. Energy Mater. Sol. Cells*, 68 (2001) 391.
19. Y. Yang,Y.M. Yang, X.Q. Du, Y. Chen and Z. Zhang, *Appl. Surf. Sci.,* 305 (2014) 330.
20. X. Huang, N. Li, H. Wang, H. Sun, S. Sun and J. Zheng, *Thin Solid Films,* 516 (2008) 1037.
21. E.A. Kulp, S.J. Limmer, E.W. Bohannan and J.A. Switzer, *Solid State Ionics,* 178 (2007) 749.

22. Y. Hamlaoui, F. Pedraza, C. Remazeilles, S. Cohendoz, C. Rébéré, L. Tifoutib and J. Creus, *Mater. Chem. Phys.,* 113 (2008) 650.
23. A. Turkovic, *J. Mater. Sci. Eng. B,* 110 (2004) 68.
24. V. Lair, A. Ringuedé, P. Vermaut and S. Griveau, *Phys. Stat. Sol. (c),* 11(2008) 3492.
25. G.R. Li, D.L Qu and Y.X. Tong, *Electrochem. Commun.,* 10 (2008) 80.
26. B.M. Reddy, P. Saikia, P. Bharali, S.E. Park, M. Muhler and W. Grunert, *J. Phys. Chem. C,* 113 (2009) 2452.
27. A. Bonnefont, R. Kostecki, F. Mclarnon, J.C. Arrayet, L. Servant and F. Argoul, *J. Electrochem. Soc.,* 149 (1999) 4101.
28. E.W. Bohannan, L.Y. Huang, F.S. Miller, M.G. Shumsky and J.A. Switzer, *Langmuir,* 15 (1999) 813.
29. F. Safizadeh, A.M. Lafront, E. Ghali and G.E. Houlachi, *J. Can. Metall. Q.* 49 (2010) 21.
30. F. Safizadeh, A.M. Lafront, E. Ghali and G.E. Houlachi, *Hydrometallurgy,* 111 (2012) 29.
31. M.F. Montemor, R. Pinto and M.G.S. Ferreira, *Electrochim. Acta,* 54 (2009) 5179.
32. C.T.J. Low and F.C. Walsh, *J. Electroanal. Chem.* 615 (2008) 95.
33. F.C. Walsh, A First Course in Electrochemical Engineering, The Electrochemical Consultancy, Romsey, 1993.
34. A.J. Bard and L.R. Faulkner, Electrochemical Methods: Fundamentals and Applications, 2nd ed., John Wiley & Sons, New York, 2001.
35. S.T. Aruna, C.N. Bindu, V. Ezhil Selvi, V.K. William Grips and K.S. Rajam, *Surf. Coat. Technol.,* 200 (2006) 6871.
36. P. Bindra and J. Tweedie, *J. Electrochem. Soc.,* 130 (1983) 1112.
37. Y.M. Yang, X.Q. Du, C.X. Yi, J. Liu and Z. Zhang, *Int. J. Electrochem. Sci.,* 12 (2017) 5304-5319.
38. A. Aballe, M. Bethencourt, F.J. Botana and M. Marcos, *Electrochem. Commun.,* 1 (1999) 266.
39. Z.H. Dong, X.P. Guo, J.S. Zheng and L.M. Xu, *Electrochem. Commun.,* 3 (2001) 561.
40. C. Cai, Z. Zhang, F.H. Cao, Z.N. Gao, J.Q. Zhang and C.N. Cao, *J. Electroana. Chem.,* 578 (2005) 143.
41. Y.Y. Shi, Z. Zhang, J.X. Su. F.H. Cao and J.Q. Zhang, *Electrochim. Acta* 51 (2006) 4977.
42. F.H. Cao, Z. Zhang, J.X. Su, Y.Y. Shi and J.Q. Zhang, *Electrochim. Acta* 51 (2006) 1359.
43. T. Zhang, Y.W. Shao, G.Z. Meng and F.H. Wang, *Electrochim. Acta,* 53 (2007) 561.
44. Z. Zhang, W.H. Leng, Q.Y. Cai, F.H. Cao and J.Q. Zhang, *J. Electroanal. Chem.,* 578 (2005) 357.
45. *M.C. Lefebvre and B.E. Conway, J. Electroana. Chem., 480 (2000) 46.*
46. X.Q. Huang, Y. Chen, T.W. Fu, Z. Zhang and J.Q. Zhang, *J. Electrochem. Soc.,* 160 (2013) D530.